Chemical Science

RSC Publishing

EDGE ARTICLE

View Article Online
View Journal

Supersized contorted aromatics†

Cite this: DOI: 10.1039/c3sc50374g

Shengxiong Xiao,‡[a] Seok Ju Kang,‡[b] Ying Wu,‡[b] Seokhoon Ahn,[be] Jong Bok Kim,[c] Yueh-Lin Loo,[c] Theo Siegrist,[d] Michael L. Steigerwald,[b] Hexing Li*[a] and Colin Nuckolls*[ab]

Received 7th February 2013
Accepted 1st March 2013

DOI: 10.1039/c3sc50374g

www.rsc.org/chemicalscience

We describe here the synthesis and electronic device properties of a new type of polycyclic aromatic molecule, the contorted octabenzocircumbiphenyl (c-OBCB). Contorted polycyclic aromatic hydrocarbons (PAHs) are promising small active molecules for organic devices. We present two different methods to synthesize c-OBCB derivatives that allow the smooth incorporation of functional groups. The material has a highly contorted exterior with six 4-helicenes and two 5-helicenes around the exterior of the expanded core of the aromatic. With appropriate sidechains, the material is soluble in common organic solvents and forms thin films. In thin films, the tetradodecyloxy-substituted c-OBCB self-assembles to form the active layer in organic field effect transistors. It is a hole transporting organic semiconductor. In the transistors, the c-OBCB forms good contact with source and drain contacts made from graphene. The c-OBCB self-assembles into a heterojunction from solution with phenyl-C_{70}-butyric acid methyl ester ($PC_{70}BM$). We observed power conversion efficiencies of ~2.9 % under 100 mW cm^{-2} illumination at a 1 : 4 weight ratio of the c-OBCB relative to $PC_{70}BM$. The c-OBCB is shape complementary to the ball shaped $PC_{70}BM$.

Here we describe the synthesis, structure, and self-assembly in electrical devices for the largest member of the contorted aromatics synthesized to date, the contorted octabenzocircumbiphenyl (c-OBCB).[1] Polycyclic aromatic hydrocarbons (PAHs) are aesthetically beautiful, synthetically challenging, and fundamentally interesting.[2] More importantly, PAHs have an increasing role as an active element in molecular electronic devices[3] such as field-effect transistors (FETs)[4] and solar cells.[5]

One strategy that we have employed when making electronic materials from PAHs is to introduce strain into their molecular structure that forces the appended rings to adopt a ruffled conformation. The peripheral groups that are bent out of the ring plane produce several advantageous consequences for the materials properties. In thin films and crystals, they are able to adopt unique π-to-π contacts that produce active materials in applications that require charge transport.[1,4c,d,6] In addition, these contorted aromatics are shape- and size-complementary to fullerenes in thin films and co-crystals. The association between contorted aromatics and fullerenes produces efficient photovoltaic cells.[7]

Until this study, we have only synthesized and tested in OPV's the smallest of this class of materials, the contorted hexabenzocoronene (c-HBC).[1,4c,d,6a,8] While the c-HBC and its derivatives are efficient in solar cells,[7] they are limited by the poor overlap of their absorption profiles with the solar spectrum.[8] Here we describe the synthesis of a new type of contorted PAH that has eight aromatic rings appended around a circumbiphenyl core (c-OBCB).

Furthermore, we describe their behavior in solar cells and thin film transistors. In transistors, the large aromatic face of the c-OBCB allows it to make efficient contact to single-layer graphene that we use as the OFET source and drain electrodes. The c-OBCB, like the c-HBC, forms a complementary structure with fullerenes and provides solar cells that are more efficient than the c-HBC.

Design

Fig. 1 shows the DFT-generated structure[9] of the lowest energy conformer of the c-OBCB. The structure is similar to the c-HBC in many respects but has some important differences. Like the c-HBC, the c-OBCB has six benzophenanthrenes arrayed around the exterior of the circumbiphenyl core. The c-OBCB has two

[a]Department of Chemistry, Optoelectronic Nano Materials and Devices Institute, Shanghai Normal University, Shanghai, China. E-mail: hexing-li@shnu.edu.cn; cn37@columbia.edu

[b]Department of Chemistry, Columbia University, New York, NY, USA

[c]Department of Chemical and Biological Engineering, Princeton University, Princeton, NJ, USA

[d]Department of Chemical and Biomedical Engineering, and National High Magnetic Field Laboratory, Tallahassee, FL, USA, 32310

[e]Institute of Advanced Composite Materials, Korea Institute of Science and Technology, Eunhari san 101, Bongdong-eup, Wanju-gun, Jeollabukdo, Republic of Korea

† Electronic supplementary information (ESI) available. CCDC reference number 923610. For ESI and crystallographic data in CIF or other electronic format see DOI: 10.1039/c3sc50374g

‡ These authors contributed equally to the work.

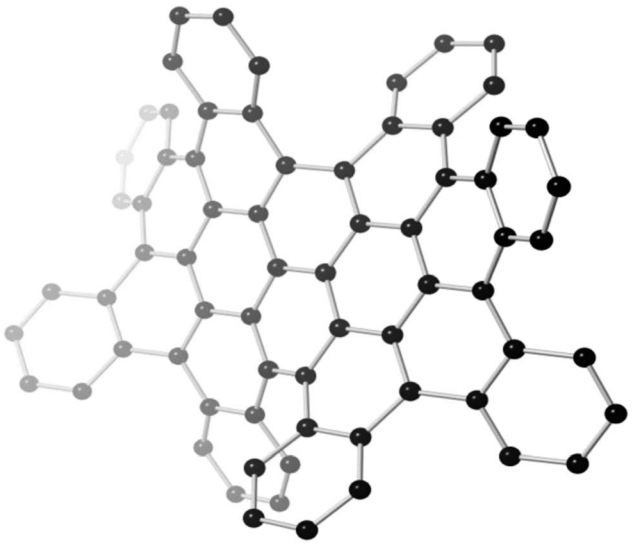

Fig. 1 The energy minimized structure from DFT calculations for c-OBCB **1a**. Hydrogens have been removed to clarify the view.

additional [5]-helicenes around its exterior. In this conformation the molecule is chiral. We found two other conformations by DFT. They are shown in the ESI (Fig. S1).† These two other geometries are essentially isoenergetic, and each is ~21 kcal mol^{-1} higher in energy than the one shown in Fig. 1.

There are no reported syntheses of circumbiphenyls except for the original 1972 Clar synthesis of the parent circumbiphenyl.[10] The harsh conditions employed in the Clar synthesis prevent using it to make functionalized derivatives. Our strategy was to synthesize the parent with solubilizing chains and to study its property in thin film devices.

Synthesis of c-OBCBs

We developed two syntheses for c-OBCB. Full synthetic details are contained in the ESI.† The key common intermediate in both syntheses is **3** shown in Scheme 1. It consists of three tetrasubstituted double bonds separated by two six-membered rings. Given the crowded structure of this tris-olefin, we grew crystals to investigate its conformational preference. Fig. 2 displays the structure obtained crystallographically. The two pentacene-like units along the short axis of the molecule are bent into opposite directions due to steric crowding. The three double bonds along the long axis of the molecule adopt a "zig–zag" conformation.

Each of the olefins **3a–c** photocyclizes to the c-OBCB skeleton under the Katz-modified Mallory photocyclization conditions (Scheme 1).[11] The yield is 83%, 80% and 82% for **1a**, **1b**, and **1c**, respectively. The derivatization of this type of c-OBCBs is simple, following our previously reported c-HBC syntheses.[1,6a] We easily include functional groups such as the solubilizing alkoxyl chains.

Scheme 2 displays the two routes we developed to produce tris-olefin (**3**) and its derivatives. Scheme 2A utilizes the thioketone (**4**) and diazoalkane (**5**) to produce coupling partners for a Barton–Kellogg olefination.[12] Using this method we were able to demonstrate that these large aromatics have unusual properties as proton sensors in thin film devices.[13]

The synthesis in Scheme 2A is step-intensive. The alternate synthesis in Scheme 2B obviates the synthesis of either the thioketone or the diazoalkane by utilizing the dione (**6**).[14] The dione is prepared in two steps from commercially available reagents.[14] Subjecting this dione to Ramirez olefination[15,16] creates the versatile tetrabromide (**7**). **7** is a yellow solid that has poor solubility in common organic solvents at room temperature, and thus can be purified simply by washing with toluene and filtering. Fortunately, compound **7** is soluble enough to allow the subsequent reactions to occur. The synthesis of the tris-olefin (**3**) can be completed easily with the Suzuki coupling[17,18] of **7** with substituted arylboronic esters.

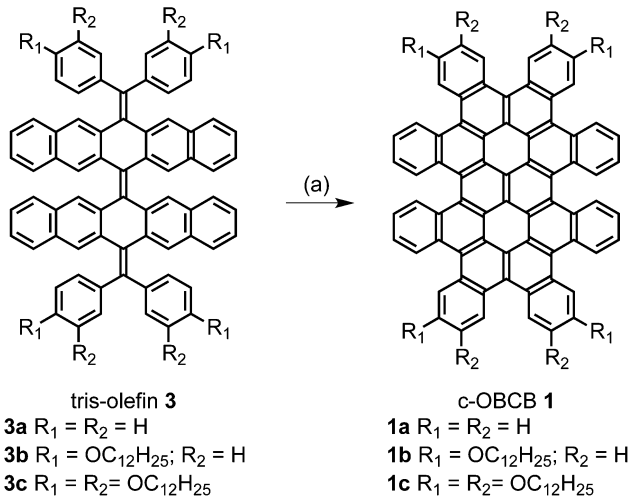

Scheme 1 The photocyclization of the tris-olefins (**3a–c**) to c-OBCBs (**1a–c**). (a) *hv*, I_2, propylene oxide, anhydrous benzene.

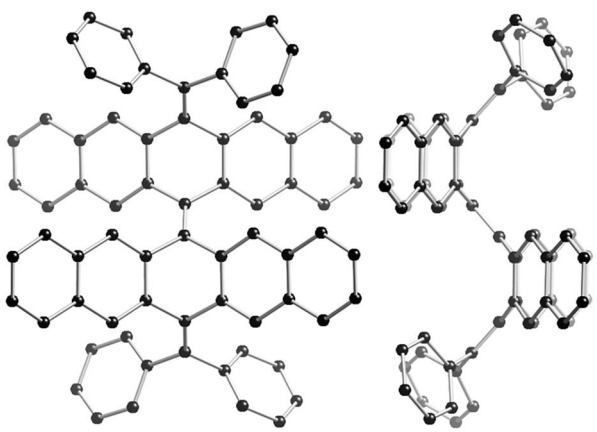

Fig. 2 Structure of tris-olefin **3a** from single-crystal X-ray diffraction. Hydrogen atoms have been removed to clarify the view. Crystals were grown by slow diffusion of methanol into a solution of **3a** in 1,2,4-trichlorobenzene.

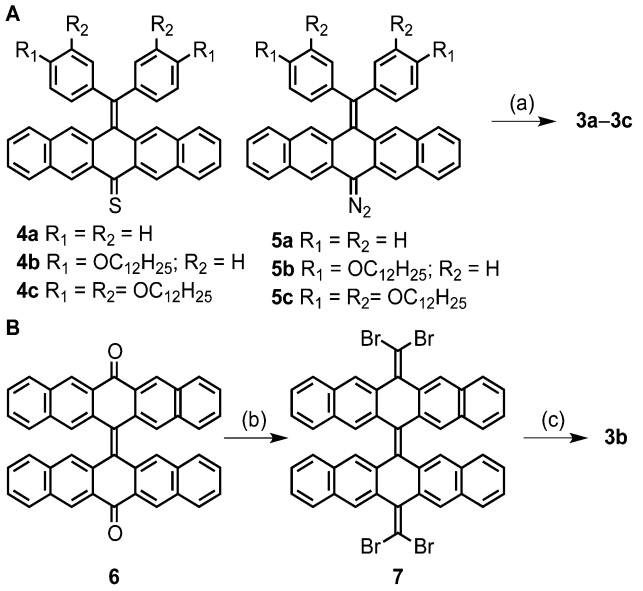

Scheme 2 Synthesis of **3** employing: (A) Barton–Kellogg olefination or (B) Ramirez olefination/Suzuki coupling sequence. (a) Dichloromethane in the dark followed by PPh_3, xylenes, reflux; (b) CBr_4, PPh_3, toluene, 80 °C; (c) substituted aryl boronic esters, $Pd(PPh_3)_4$, Na_2CO_3, DME/H_2O, 100 °C.

Molecular and materials characterization

The unsubstituted c-OBCB (**1a**) is a red powder that has limited solubility in common organic solvents (~10 mg mL^{-1} in 1,1,2,2-tetrachloroethane). It precipitates from the benzene solution upon the completion of the photocyclization. We synthesized derivatives **1b** with four sidechains because the corresponding c-HBC forms a columnar liquid crystalline film that acts as a p-type organic semiconductor.[1] The c-HBC that corresponds to **1c** with eight sidechains forms nanoscale cables that can be placed in devices.[6a]

As expected the sidechains drastically increase solubility. **1b** and **1c** have a solubility of over 100 mg mL^{-1} and 200 mg mL^{-1} in chloroform, respectively. The melting point decreased dramatically with dodecyloxy substitution on the c-OBCB core. **1a** melts above 550 °C. **1b** melts below 200 °C. **1b** forms rod-like nanostructure from mixtures of methylene chloride and methanol. **1c** is a waxy-oil that melts near room temperature.

Fig. 3 displays the UV-visible (UV-vis) and photoluminescence (PL) spectra of **1b** in *o*-xylene at ~10^{-6} M. It shows strong absorbance at 411 nm, 433 nm and 493 nm. The strong absorptions below 350 nm are due to the pendant phenyl groups. The peaks at 411 nm and 433 nm are the β-bands of c-OBCB. The peak at 493 nm is the p-band. The weak absorptions at 550 nm are most likely due to (radialene π)–(radialene π*) triplets. The assignment of these transitions to a triplet state is supported by the PL spectrum shown in Fig. 3. Moreover, transition moment calculations show that the lowest-energy excitations are strongly allowed. So, weak absorptions must be due to otherwise forbidden processes. The fluorescence spectra collected by excitation at 433 nm showed two strong emission peaks at 549 nm and 593 nm, along with a small peak at 645 nm.

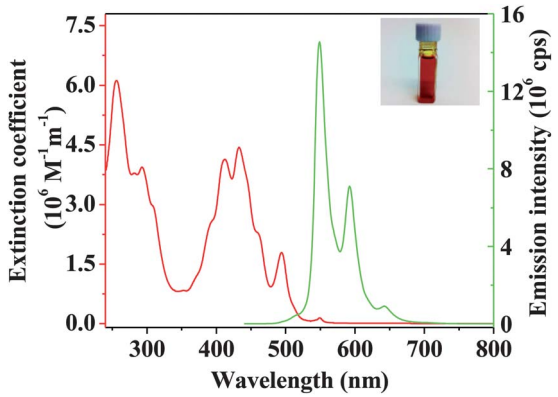

Fig. 3 UV-vis (red) and fluorescence (green curve, excited at 433 nm) spectroscopy of c-OBCB **1b** in *o*-xylene at ~10^{-6} M concentration with a path length of l = 1 cm. The inset shows a 5 mM solution of **1b** in chloroform.

The absorbance and emission maxima for the c-OBCBs are red-shifted by ~65 nm when compared to the smaller c-HBCs.[8]

Characterization in OFETs

We created OFETs from the c-OBCB **1b** in a device where the source, drain, and active layer were transfer printed. We use graphene source and drain contacts that were pattern transfer printed using a process we described earlier.[19] The c-OBCB solution in *o*-xylene solvent was spin cast onto 20 μm lines patterned in a PDMS mold that was transferred onto the graphene electrodes on a silicon wafer with 300 nm of silicon oxide on its surface. The silicon serves as a global back gate for the

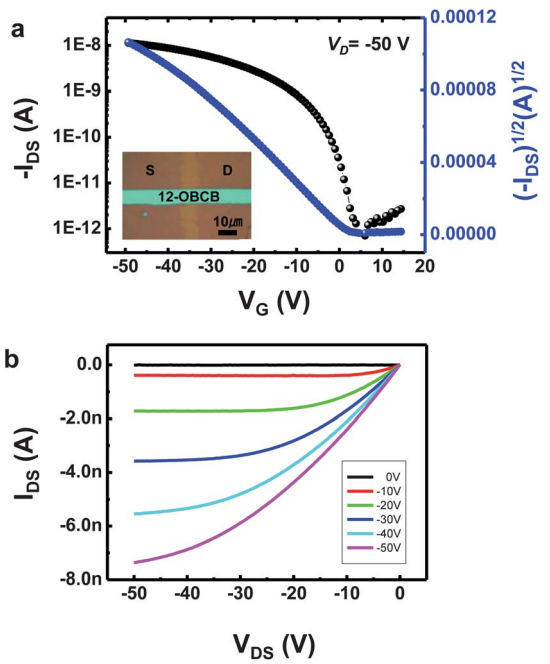

Fig. 4 Transfer (a) and output (b) curve of patterned c-OBCB **1b** transistor. Inset of (a) shows an optical microscope image of c-OBCB **1b** channel bridged between CVD-graphene S/D.

devices. The inset in Fig. 4 shows the active layer located between a pair of graphene electrodes. The important point is that both the active layer of the c-OBCB and the graphene electrodes can be transfer printed in the working devices.

Fig. 4a and b display the transfer and output characteristics of the OFET. We calculate the field effect mobility from the transfer characteristics (Fig. 4a) to be 0.002 $cm^2\ V^{-1}\ s^{-1}$.[20] Fig. 4b shows the representative output characteristics of the OFET with increasing gate field (Fig. 4b). The film displays an increase of I_{DS} with negative gate bias due to the accumulation of holes in the molecular film; thus c-OBCB **1b** transports holes readily. The micropatterned c-OBCB film reduces the gate leakage current and operates well with the single layer graphene electrodes. In addition, the graphene S/D electrodes provide very low contact resistance with the c-OBCB film as seen in the low bias region of Fig. 4a. The low contact resistance is due to the large PAH making good contact to graphene electrodes and to the intrinsic work function adjustment of graphene.[21]

Characterization in OPVs

Our previous studies on the contorted aromatics in solar cells[7] have shown that a specific association between the donor and acceptor is important for efficacious devices spun from solution.[7] We mix the c-OBCB **1b** with varying amounts of the n-type phenyl-C_{70}-butyric acid methyl ester ($PC_{70}BM$). We suppose that the curved structure of the c-OBCB will be able to make a ball and socket interaction with the convex guest. Stern–Volmer analysis[22] of the fluorescence quenching reveals an association constant of $\sim 5 \times 10^4\ M^{-1}$ in chloroform. The data is contained in the ESI (Fig. S2†).

We next test whether the **1b**/$PC_{70}BM$ complex when cast into films would form the active layer in a photovoltaic device. We measure the HOMO and LUMO levels of the c-OBCB using cyclic voltammetry in Fig. S3† with a ferrocene standard. The c-OBCB **1b**:$PC_{70}BM$ mixture solution (solvent: *o*-xylene) was spin cast on the top of ~30 nm PEDOT:PSS/ITO substrate. Fig. 5a shows the energy diagram of each layer in the final device architecture. A TiO_x layer was employed on the top of the c-OBCB **1b**:$PC_{70}BM$ layer prior to evaporation of ~60 nm aluminum counter electrode.[23] We tested several ratios of the donor and acceptor and found optimal performance at 1 : 4 weight ratio of the donor to acceptor (see ESI, Fig. S4† for results based on other ratios). Fig. 5b displays the *J*–*V* curves for the blended films. The open circuit voltage (V_{oc}) is 0.98 V and very close to what would be predicted theoretically from the energy level alignment in Fig. 5a. The short-circuit current (J_{sc}) is 7.9 mA cm^{-2} and the fill factor is 0.37. These values result in a 2.88% power conversion efficiency. The average value is 2.86% from twelve devices. The external quantum efficiency (EQE) spectra in Fig. 5c shows the photocurrent response of c-OBCB **1b**:$PC_{70}BM$ solar cell devices as a function of wavelengths. We observe a red shifted maximum wavelength in EQE spectra compared with contorted c-HBC and its derivatives.[7] The red-shift in absorbance is responsible for the higher PCE for c-OBCB compared to the smaller c-HBC series and charts a clear path to improving the properties of these materials in OPVs by further red-shifting the absorbance.

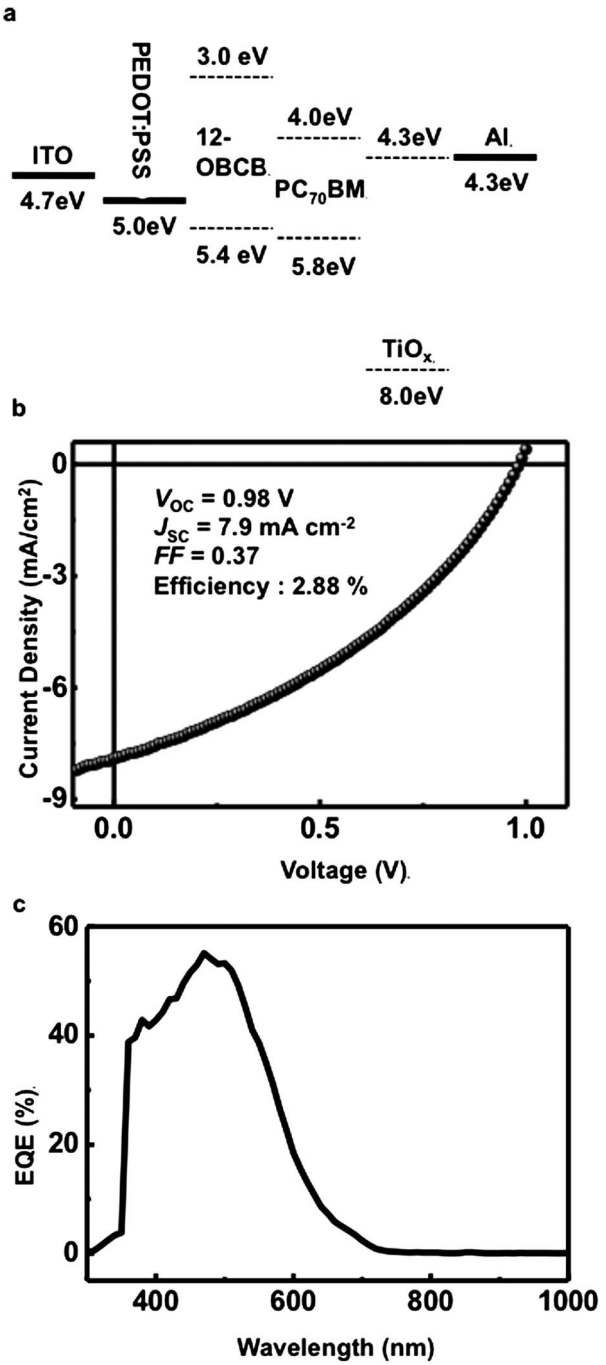

Fig. 5 (a) Energy level diagram of the device. Current density–voltage (*J*–*V*) characteristics (b) and EQE spectrum (c) of c-OBCB **1b**:$PC_{70}BM$ solar cell.

Conclusion

We describe here the synthesis and electronic device properties of a new type of polycyclic aromatic molecule. We reveal two different methods to synthesize c-OBCB derivatives that allow the smooth incorporation of functional groups. The material has a highly contorted exterior with six 4-helicenes and two 5-helicenes around the exterior of the expanded core of the aromatic. With appropriate sidechains, the material is soluble in common organic solvents and forms thin films. The tetradodecyloxy-substituted

c-OBCB self-assembles to form the active layer in organic field effect transistors. The c-OBCB also self-assembles into a heterojunction from solution with $PC_{70}BM$.

Acknowledgements

Design synthesis, OFET characterization, and initial OPV properties were performed at Columbia University as part of the Center for Re-Defining Photovoltaic Efficiency through Molecular Scale Control, an Energy Frontier Research Center funded by the U.S. Department of Energy, Office of Science, Office of Basic Energy Science under Award Number DE-SC0001085. OPV characterization was performed at Princeton University, supported by the Photovoltaics Program at ONR (N00014-11010328), and the SOLAR Initiative at the NSF (DMR-1035217), and an NSF sponsored MRSEC through Princeton Center for Complex Materials (DMR-0819860). Crystal structure determination was performed at the National Magnetic Field Laboratory which is supported by the National Science Foundation Cooperative Agreement (DMR-1157490), the State of Florida, and the U.S. Department of Energy.

Notes and references

1 S. Xiao, M. Myers, Q. Miao, S. Sanaur, K. Pang, M. L. Steigerwald and C. Nuckolls, *Angew. Chem., Int. Ed.*, 2005, **44**, 7390–7394.

2 (*a*) A. C. Grimsdale and K. Müllen, *Angew. Chem., Int. Ed.*, 2005, **44**, 5592–5629; (*b*) B. Hajgató, M. S. Deleuze and K. Ohno, *Chem.–Eur. J.*, 2006, **12**, 5757–5769; (*c*) B. Hajgató and K. Ohno, *Chem. Phys. Lett.*, 2004, **385**, 512–518; (*d*) S. Müller and K. Müllen, *Philos. Trans. R. Soc. London, Ser. A*, 2007, **365**, 1453–1472; (*e*) V. Palermo, S. Morelli, C. Simpson, K. Mullen and P. Samori, *J. Mater. Chem.*, 2006, **16**, 266–271; (*f*) D. F. Rohlfing and A. Kuhn, *Carbon*, 2006, **44**, 1942–1948; (*g*) X. Shen, D. M. Ho and R. A. Pascal, *J. Am. Chem. Soc.*, 2004, **126**, 5798–5805; (*h*) C. D. Simpson, J. D. Brand, A. J. Berresheim, L. Przybilla, H. J. Räder and K. Müllen, *Chem.–Eur. J.*, 2002, **8**, 1424–1429; (*i*) D. Wasserfallen, M. Kastler, W. Pisula, W. A. Hofer, Y. Fogel, Z. Wang and K. Müllen, *J. Am. Chem. Soc.*, 2006, **128**, 1334–1339; (*j*) J. Wu, Ž. Tomović, V. Enkelmann and K. Müllen, *J. Org. Chem.*, 2004, **69**, 5179–5186; (*k*) X. Feng, J. Wu, M. Ai, W. Pisula, L. Zhi, J. P. Rabe and K. Müllen, *Angew. Chem., Int. Ed.*, 2007, **46**, 3033–3036; (*l*) W. Pisula, M. Kastler, D. Wasserfallen, J. W. F. Robertson, F. Nolde, C. Kohl and K. Müllen, *Angew. Chem., Int. Ed.*, 2006, **45**, 819–823; (*m*) J. P. Schmidtke, R. H. Friend, M. Kastler and K. Mullen, *J. Chem. Phys.*, 2006, **124**, 174704–174706; (*n*) J. Wu, M. Baumgarten, M. G. Debije, J. M. Warman and K. Müllen, *Angew. Chem., Int. Ed.*, 2004, **43**, 5331–5335; (*o*) S. Pogodin and I. Agranat, *Org. Lett.*, 1999, **1**, 1387–1390.

3 J. Wu, W. Pisula and K. Müllen, *Chem. Rev.*, 2007, **107**, 718–747.

4 (*a*) T. Mori, H. Takeuchi and H. Fujikawa, *J. Appl. Phys.*, 2005, **97**, 066102–066103; (*b*) M. Kastler, F. Laquai, K. Mullen and G. Wegner, *Appl. Phys. Lett.*, 2006, **89**, 252103–252103; (*c*) X. Guo, M. Myers, S. Xiao, M. Lefenfeld, R. Steiner, G. S. Tulevski, J. Tang, J. Baumert, F. Leibfarth, J. T. Yardley, M. L. Steigerwald, P. Kim and C. Nuckolls, *Proc. Natl. Acad. Sci. U. S. A.*, 2006, **103**, 11452–11456; (*d*) J. Luo, X. Xu, R. Mao and Q. Miao, *J. Am. Chem. Soc.*, 2012, **134**, 13796.

5 (*a*) L. Schmidt-Mende, A. Fechtenkotter, K. Mullen, E. Moons, R. H. Friend and J. D. MacKenzie, *Science*, 2001, **293**, 1119–1122; (*b*) J. Jung, A. Rybak, A. Slazak, S. Bialecki, P. Miskiewicz, I. Glowacki, J. Ulanski, S. Rosselli, A. Yasuda, G. Nelles, Ž. Tomović, M. D. Watson and K. Müllen, *Synth. Met.*, 2005, **155**, 150–156; (*c*) L. Schmidt-Mende, A. Fechtenkötter, K. Müllen, R. H. Friend and J. D. MacKenzie, *Phys. E.*, 2002, **14**, 263–267.

6 (*a*) S. Xiao, J. Tang, T. Beetz, X. Guo, N. Tremblay, T. Siegrist, Y. Zhu, M. Steigerwald and C. Nuckolls, *J. Am. Chem. Soc.*, 2006, **128**, 10700–10701; (*b*) X. Guo, S. Xiao, M. Myers, Q. Miao, M. L. Steigerwald and C. Nuckolls, *Proc. Natl. Acad. Sci. U. S. A.*, 2009, **106**, 691–696.

7 (*a*) T. Schiros, S. Mannsfeld, C.-Y. Chiu, K. G. Yager, J. Ciston, A. A. Gorodetsky, M. Palma, Z. Bullard, T. Kramer, D. Delongchamp, D. Fischer, I. Kymissis, M. F. Toney and C. Nuckolls, *Adv. Funct. Mater.*, 2012, **22**, 1167–1173; (*b*) S. J. Kang, J. B. Kim, C.-Y. Chiu, S. Ahn, T. Schiros, S. S. Lee, K. G. Yager, M. F. Toney, Y.-L. Loo and C. Nuckolls, *Angew. Chem., Int. Ed.*, 2012, **51**, 8594–8597; (*c*) N. J. Tremblay, A. A. Gorodetsky, M. P. Cox, T. Schiros, B. Kim, R. Steiner, Z. Bullard, A. Sattler, W.-Y. So, Y. Itoh, M. F. Toney, H. Ogasawara, A. P. Ramirez, I. Kymissis, M. L. Steigerwald and C. Nuckolls, *ChemPhysChem*, 2010, **11**, 799–803; (*d*) A. A. Gorodetsky, C.-Y. Chiu, T. Schiros, M. Palma, M. Cox, Z. Jia, W. Sattler, I. Kymissis, M. Steigerwald and C. Nuckolls, *Angew. Chem., Int. Ed.*, 2010, **49**, 7909–7912.

8 Y. S. Cohen, S. Xiao, M. L. Steigerwald, C. Nuckolls and C. R. Kagan, *Nano Lett.*, 2006, **6**, 2838–2841.

9 X. Gonze, J. M. Beuken, R. Caracas, F. Detraux, M. Fuchs, G. M. Rignanese, L. Sindic, M. Verstraete, G. Zerah, F. Jollet, M. Torrent, A. Roy, M. Mikami, P. Ghosez, J. Y. Raty and D. C. Allan, *Comput. Mater. Sci.*, 2002, **25**, 478–492.

10 E. Clar and C. C. Mackay, *Tetrahedron*, 1972, **28**, 6041–6047.

11 L. Liu, B. Yang, T. J. Katz and M. K. Poindexter, *J. Org. Chem.*, 1991, **56**, 3769–3775.

12 (*a*) D. H. R. Barton, E. H. Smith and B. J. Willis, *J. Chem. Soc. D*, 1970, 1226; (*b*) D. H. R. Barton and B. J. Willis, *J. Chem. Soc. D*, 1970, 1225–1226; (*c*) J. Buter, S. Wassenaar and R. M. Kellogg, *J. Org. Chem.*, 1972, **37**, 4045–4060.

13 The synthetic details for **1b**, **3b**, **4b**, and **5b** using the Barton–Kellogg procedure can be found in: S. Xiao, S. J. Kang, Y. Zhong, S. Zhang, A. Scott, A. Moscatelli, N. Turro, M. L. Steigerwald, H. Li and C. Nuckolls, *Angew. Chem., Int. Ed.*, 2013, in press.

14 X. Zhang, X. Jiang, J. Luo, C. Chi, H. Chen and J. Wu, *Chem.–Eur. J.*, 2010, **16**, 464–468.

15 N. B. Desai, N. McKelvie and F. Ramirez, *J. Am. Chem. Soc.*, 2002, **84**(9), 1745–1747.
16 K. N. Plunkett, K. Godula, C. Nuckolls, N. Tremblay, A. C. Whalley and S. Xiao, *Org. Lett.*, 2009, **11**(11), 2225–2228.
17 N. Miyaura and A. Suzuki, *Chem. Rev.*, 1995, **95**(7), 2457–2483.
18 A. Bauer, M. W. Miller, S. F. Vice and S. W. McCombie, *Synlett*, 2001, **2**, 254–256.
19 S. J. Kang, B. Kim, K. S. Kim, Y. Zhao, Z. Chen, G. H. Lee, J. Hone, P. Kim and C. Nuckolls, *Adv. Mater.*, 2011, **23**, 3531–3535.
20 We use the MOSFET standard model in the saturated regime, $I_{DS} = (W/2L)C_i\mu(V_G - V_T)^2$. W and L are the width and length of channel and C_i, μ, and V_T correspond to the capacitance per unit area of the gate insulator, the field-effect mobility and threshold voltage, respectively.
21 Y.-J. Yu, Y. Zhao, S. Ryu, L. E. Brus, K. S. Kim and P. Kim, *Nano Lett.*, 2009, **9**, 3430–3434.
22 O. Stern and M. Volmer, *Zeitschrift für Physik Z*, 1919, **20**, 183–188.
23 The current density–voltage (J–V) characteristic of devices was acquired using a Keithley 2635 source measurement unit under 100 mW cm^{-2} illumination.